Synthesis and Characterization of Ni-Doped $ZnFe_2O_4$ Nanocomposites via Chemical Co-precipitation Method

Ningurkar A. D[1], Bajpeyee A. U[2]
[1,2]*Research Centre in Physics, Smt. Narsamma ACS College, Kiran Nagar, Amravati (MS), India 444606*
doi.org/10.64643/IJIRTV12I9-195645-459

***Abstract*—Ni-doped $ZnFe_2O_4$ nanocomposites with nickel concentrations of 0.1, 0.3, and 0.5 wt% were synthesized using a chemical co-precipitation technique. Structural, morphological, elemental and optical characterizations were performed to study the effect of Ni incorporation. XRD analysis confirmed the formation of a single-phase cubic spinel structure, while peak shifts and crystallite size variations indicated successful substitution of Ni^{2+} ions into the $ZnFe_2O_4$ lattice. FTIR spectra showed characteristic metal-oxygen vibrations associated with tetrahedral and octahedral sites. FE-SEM and EDS analyses revealed agglomerated nanostructures with homogeneous elemental distribution. UV–Visible spectroscopy demonstrated band gap variation with increasing Ni content due to lattice distortion and electronic structure changes. The results demonstrate that Ni doping effectively tailors the properties of $ZnFe_2O_4$ nanocomposites.**

***Index Terms*—Ni-doped $ZnFe_2O_4$; Co-precipitation; Spinel ferrite; Nanocomposites.**

I. INTRODUCTION

Spinel ferrites with the general formula MFe_2O_4 (where M represents a divalent metal ion such as Zn^{2+}, Ni^{2+}, Co^{2+}, Mn^{2+}, etc.) constitute an important class of magnetic oxide nanomaterials due to their remarkable structural versatility, chemical stability, and tunable physicochemical properties [1-2]. These materials crystallize in a cubic close-packed oxygen lattice belonging to the Fd3m space group, where metal cations occupy tetrahedral (A) and octahedral (B) interstitial sites. The distribution of cations between these sites governs the magnetic, electrical, optical, and catalytic properties of the ferrite system [3-4].

Among various spinel ferrites, $ZnFe_2O_4$ has attracted extensive research interest because of its unique semiconducting nature, moderate band gap, environmental compatibility, and multifunctional behaviour [5-6]. In its bulk form, $ZnFe_2O_4$ typically exhibits a normal spinel structure in which Zn^{2+} ions preferentially occupy tetrahedral (A) sites while Fe^{3+} ions occupy octahedral (B) sites [7]. However, at the nanoscale, partial inversion of cations can occur, leading to significant deviations in magnetic and electronic behavior. Such size-induced and synthesis-dependent cation redistribution makes $ZnFe_2O_4$ particularly attractive for property engineering.

$ZnFe_2O_4$ nanomaterials have been widely explored for applications in photocatalysis, gas sensing, lithium-ion batteries, electromagnetic devices, environmental remediation, and biomedical fields [8]. Nevertheless, pure $ZnFe_2O_4$ often exhibits limitations such as low magnetization, restricted electrical conductivity, and moderate catalytic efficiency. Therefore, strategic modification through transition metal doping has emerged as an effective approach to enhance its functional performance.

Nickel (Ni^{2+}) is a promising dopant for $ZnFe_2O_4$ due to its strong preference for octahedral (B) sites and its intrinsic magnetic moment [9]. Substitution of Ni^{2+} into the $ZnFe_2O_4$ lattice introduces several important effects, especially, modification of cation distribution between A and B sites, alteration of super-exchange interactions (A–B and B–B interactions), variation in lattice parameters due to differences in ionic radii (Ni^{2+} ≈ 0.69 Å; Zn^{2+} ≈ 0.74 Å), enhancement in magnetic and electrical properties, improved crystallinity and structural stability. Ni substitution often transforms the normal spinel structure toward a partially inverse spinel configuration. This cation redistribution directly influences magnetic exchange interactions between Fe^{3+}–O^{2-}–Fe^{3+} and Ni^{2+}–O^{2-}–Fe^{3+} linkages, thereby modifying the overall magnetic ordering and physicochemical behaviour of the ferrite system [10].

Various synthesis methods have been employed for preparing Ni-doped $ZnFe_2O_4$ nanostructures, including sol–gel, hydrothermal, combustion,

microwave-assisted synthesis, and solid-state reaction [11]. However, many of these methods involve high processing temperatures, long reaction times, or complex experimental setups. In contrast, chemical co-precipitation is widely recognized as a simple, cost-effective, and scalable technique that offers excellent control over stoichiometry, particle size, and homogeneity. The method operates under relatively mild conditions and enables uniform nucleation and growth of nanoparticles through controlled precipitation at alkaline pH.

In the co-precipitation process, metal cations are simultaneously precipitated as hydroxides under controlled pH conditions, followed by thermal treatment to induce crystallization of the spinel phase. Key synthesis parameters such as pH, temperature, aging time, stirring rate, and calcination temperature play critical roles in determining the structural and morphological characteristics of the final nanomaterials. Maintaining a highly alkaline medium (pH 10–11) ensures complete precipitation of metal hydroxides and promotes homogeneous cation distribution prior to spinel formation [12].

Although several reports exist on Ni–Zn ferrite systems, systematic investigation of controlled nickel substitution levels (x = 0.1, 0.3, 0.5) synthesized under identical co-precipitation conditions remains essential to clearly understand compositional influence on structural evolution [13]. Comparative evaluation across multiple doping concentrations provides deeper insight into lattice distortion, crystallite size variation, and possible cation redistribution mechanisms.

Therefore, the present study focuses on the synthesis of $Ni_xZn_{1-x}Fe_2O_4$ (x = 0.0, 0.1, 0.3, 0.5) nanocomposites via a controlled chemical co-precipitation method followed by calcination. The objective is to systematically examine the effect of increasing Ni^{2+} concentration on the structural framework of $ZnFe_2O_4$ spinel ferrite nanomaterials. The adopted synthesis strategy ensures compositional precision, phase purity, and reproducibility, making it suitable for scalable production of doped ferrite nanostructures for advanced technological applications.

II. MATERIALS AND METHODS

A. Materials:

All chemicals used in the present study were of analytical reagent (AR) grade and employed without further purification. Ferric nitrate nonahydrate ($Fe(NO_3)_3 \cdot 9H_2O$), zinc nitrate hexahydrate ($Zn(NO_3)_2 \cdot 6H_2O$), nickel nitrate hexahydrate ($Ni(NO_3)_2 \cdot 6H_2O$), and sodium hydroxide (NaOH) pellets were used as received. Distilled/deionized (DI) water was used throughout the synthesis process. All glassware was thoroughly cleaned with dilute nitric acid, rinsed repeatedly with DI water, and dried prior to use to avoid contamination and ensure compositional accuracy.

B. Stoichiometric Design and Synthesis of $Ni_xZn_{1-x}Fe_2O_4$ Nanocomposites

Nickel-doped zinc ferrite nanocomposites with the general formula $Ni_xZn_{1-x}Fe_2O_4$ (x = 0.0, 0.1, 0.3, and 0.5) were synthesized via a controlled chemical co-precipitation method. The molar ratio of divalent to trivalent cations was maintained according to spinel stoichiometry, such that $(Ni^{2+} + Zn^{2+}) : Fe^{3+} = 1 : 2$. The precursor quantities were calculated precisely to satisfy the required molar fractions of Ni^{2+} and Zn^{2+} substitution while maintaining phase purity of the cubic spinel structure [14].

For the synthesis of pure $ZnFe_2O_4$ (x = 0.0), 12.35 g of $Zn(NO_3)_2 \cdot 6H_2O$ and 33.52 g of $Fe(NO_3)_3 \cdot 9H_2O$ were dissolved separately in approximately 80 mL and 160 mL of DI water, respectively. The solutions were combined under continuous magnetic stirring at 600–900 rpm, and the total volume was adjusted to about 300 mL. For Ni-substituted compositions, stoichiometric amounts of nickel nitrate hexahydrate were incorporated while proportionally reducing zinc nitrate to maintain the overall divalent cation concentration constant. Specifically, for $Ni_{0.1}Zn_{0.9}Fe_2O_4$, 33.60 g $Fe(NO_3)_3 \cdot 9H_2O$, 11.13 g $Zn(NO_3)_2 \cdot 6H_2O$, and 1.209 g $Ni(NO_3)_2 \cdot 6H_2O$ were used. For $Ni_{0.3}Zn_{0.7}Fe_2O_4$, 33.789 g $Fe(NO_3)_3 \cdot 9H_2O$, 8.707 g $Zn(NO_3)_2 \cdot 6H_2O$, and 3.646 g $Ni(NO_3)_2 \cdot 6H_2O$ were taken. Similarly, for $Ni_{0.5}Zn_{0.5}Fe_2O_4$, 33.983 g $Fe(NO_3)_3 \cdot 9H_2O$, 6.256 g $Zn(NO_3)_2 \cdot 6H_2O$, and 6.115 g $Ni(NO_3)_2 \cdot 6H_2O$ were employed. Each metal salt was dissolved separately in DI water and then added sequentially under controlled stirring at 30–40 °C to

ensure homogeneous mixing of metal cations at the molecular level.

A 1.0 M NaOH solution was prepared by dissolving 14.0 g NaOH pellets in approximately 300 mL DI water under continuous cooling due to the exothermic nature of dissolution, and the final volume was adjusted to 350 mL. The alkaline solution was added dropwise to the mixed metal nitrate solution under vigorous magnetic stirring while carefully maintaining the pH between 10 and 11. The controlled addition, typically completed within 10–30 minutes, ensured uniform nucleation and simultaneous precipitation of metal hydroxides. At this alkaline pH, Zn^{2+}, Ni^{2+}, and Fe^{3+} ions precipitate as their respective hydroxides according to:

$Zn^{2+} + 2OH^- \rightarrow Zn(OH)_2$

$Ni^{2+} + 2OH^- \rightarrow Ni(OH)_2$

$Fe^{3+} + 3OH^- \rightarrow Fe(OH)_3$

The resulting mixed hydroxide precipitate provides a homogeneous precursor for spinel ferrite formation. After achieving the desired pH, the reaction mixture was heated to 80 °C and aged under continuous stirring for 3 hours to promote complete precipitation, enhanced nucleation, and uniform cation redistribution. The pH was periodically monitored and adjusted, if necessary, to remain near 10 to prevent incomplete precipitation or formation of secondary phases.

Following aging, the slurry was allowed to cool to room temperature and centrifuged at 6000–8000 rpm for approximately 10 minutes to separate the precipitate. The collected solid was washed repeatedly (3–5 times) with DI water until the supernatant reached neutral pH (≈7), ensuring removal of residual sodium and nitrate ions. An optional ethanol wash was performed to facilitate rapid drying and reduce agglomeration. The purified precipitate was then dried in a hot air oven at 80 °C for 12 hours to remove physically adsorbed moisture.

The dried precursor powder was finally calcined in an alumina crucible at 700 °C for 3 hours in a muffle furnace to induce crystallization of the cubic spinel phase. During calcination, the metal hydroxides undergo dehydration and solid-state diffusion to form the thermodynamically stable $Ni_xZn_{1-x}Fe_2O_4$ spinel structure. The overall formation reaction can be represented as:

$Ni^{2+} + Zn^{2+} + 2Fe^{3+} + 8OH^- \rightarrow Ni_xZn_{1-x}Fe_2O_4 + 4H_2O$

The controlled stoichiometry, alkaline precipitation conditions, and thermal treatment collectively ensured formation of homogeneous, phase-pure Ni-doped $ZnFe_2O_4$ nanocomposites suitable for structural and functional investigations.

III. RESULTS AND DISCUSSION

A. XRD Analysis

The X-ray diffraction patterns of pure $ZnFe_2O_4$ and Ni-doped $ZnFe_2O_4$ (x = 0.1, 0.3, 0.5) nanocomposites exhibit well-defined diffraction peaks corresponding to the cubic spinel ferrite structure (Figure 1a). The prominent diffraction peaks observed at $2\theta \approx 30°$, 35°, 37°, 43°, 53°, 57°, 63°, 74°, and 79° can be indexed to the crystallographic planes (220), (311), (222), (400), (422), (511), (440), (533), and (622), respectively, which are characteristic reflections of the face-centered cubic spinel structure (space group Fd3m) [15].

The most intense peak corresponding to the (311) plane confirms the formation of a well-crystallized spinel phase. No additional impurity peaks related to secondary phases such as NiO, ZnO, or Fe_2O_3 were detected, indicating successful incorporation of Ni^{2+} ions into the $ZnFe_2O_4$ lattice without altering the phase purity.

With increasing Ni concentration, slight changes in peak intensity and minor shifts in peak position are observed. These variations may be attributed to lattice distortion caused by substitution of Zn^{2+} (ionic radius ≈ 0.74 Å) with comparatively smaller Ni^{2+} ions (≈ 0.69 Å). Such substitution induces modification in lattice parameter and cation distribution between tetrahedral (A) and octahedral (B) sites. The gradual sharpening of peaks with higher Ni content suggests improved crystallinity due to enhanced nucleation and crystal growth during calcination.

The nanocrystalline nature of the samples is confirmed by the noticeable peak broadening. The average crystallite size (D) can be estimated using the Debye–Scherrer equation:

$$D = \frac{0.9\lambda}{\beta \cos\theta}$$

where λ is the X-ray wavelength, β is the full width at half maximum (FWHM), and θ is the Bragg angle. The observed broadening confirms formation of nanoscale ferrite particles.

Overall, XRD analysis confirms the successful synthesis of phase-pure cubic $Ni_xZn_{1-x}Fe_2O_4$ nanocomposites.

B. FTIR Analysis

The FTIR spectra recorded in the range 4000–400 cm^{-1} provide information about functional groups and metal–oxygen bonding in the spinel structure (Figure 1b) [16].

The broad absorption band observed around ~3519 cm^{-1} corresponds to O–H stretching vibrations of adsorbed water molecules and surface hydroxyl groups. The band near ~1644 cm^{-1} is attributed to H–O–H bending vibrations of physically adsorbed moisture.

The absorption bands around ~1459 cm^{-1} and ~1379 cm^{-1} are associated with residual nitrate groups or C–O stretching vibrations, indicating trace remnants from precursor salts.

The most significant characteristic features of spinel ferrites are observed in the lower wavenumber region. The strong absorption band near ~712 cm^{-1} corresponds to intrinsic metal–oxygen stretching vibrations at tetrahedral (A) sites, while the band around ~496 cm^{-1} is attributed to metal–oxygen vibrations at octahedral (B) sites.

The presence of these two distinct absorption bands confirms the formation of the spinel ferrite structure. Slight shifts in these bands with increasing Ni content suggest modification of metal–oxygen bond strength and redistribution of cations between A and B sites due to Ni^{2+} substitution. Since Ni^{2+} preferentially occupies octahedral sites, changes in the octahedral vibration band further support successful incorporation of nickel into the lattice.

Thus, FTIR results corroborate the XRD findings and confirm formation of the spinel ferrite framework.

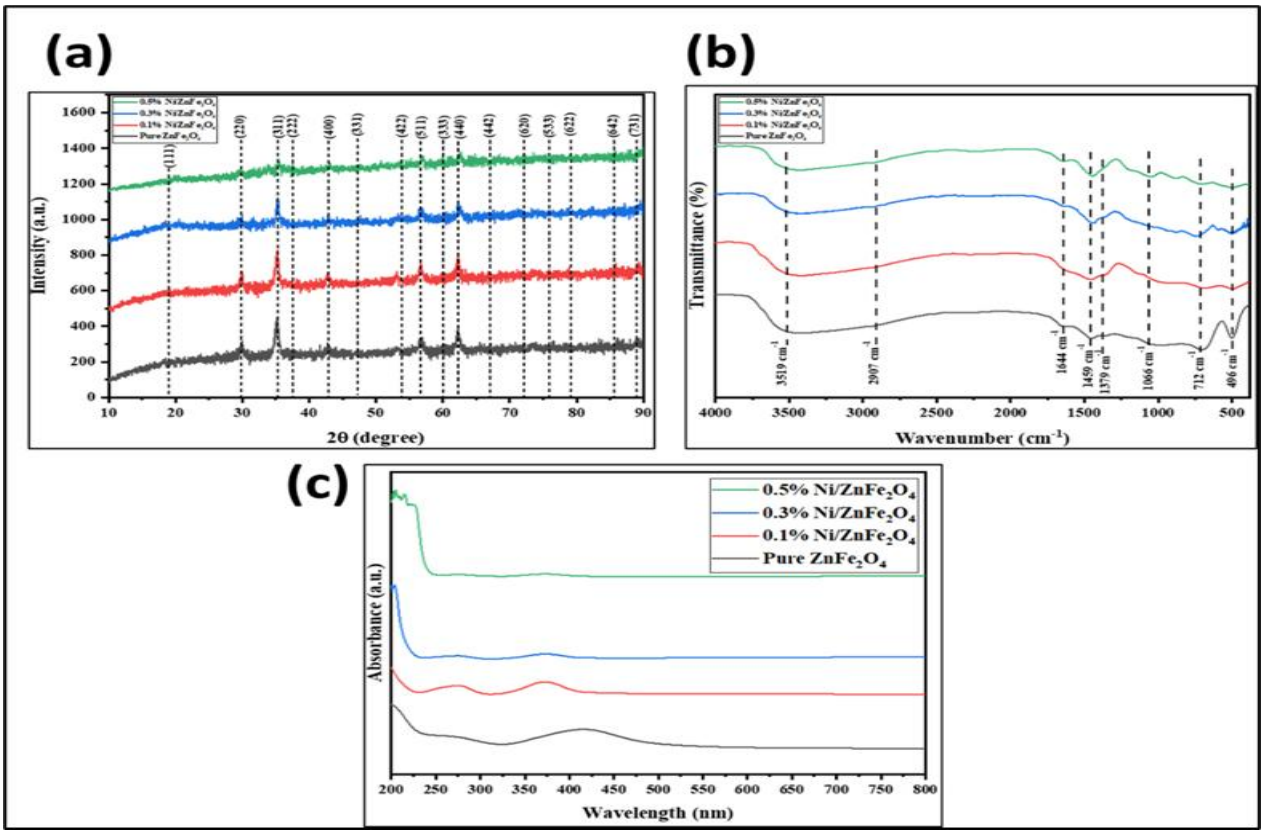

Figure 1. (a) X-ray diffraction (XRD) patterns, (b) Fourier transform infrared (FTIR) spectra, and (c) UV–Visible absorption spectra of pure $ZnFe_2O_4$ and Ni-doped $ZnFe_2O_4$ nanocomposites ($Ni_xZn_{1-x}Fe_2O_4$, x = 0.1, 0.3, 0.5) synthesized via chemical co-precipitation method.

C. UV–Visible Spectral Analysis

The UV–Visible absorption spectra recorded in the wavelength range 200–800 nm reveals the optical behaviour of pure and Ni-doped $ZnFe_2O_4$ nanocomposites (Figure 1c) [17]. All samples exhibit strong absorption in the UV region followed by a

gradual decrease toward the visible region, characteristic of ferrite semiconductors. The absorption edge appears in the near-UV to visible region, indicating semiconducting nature of the materials. A noticeable enhancement in absorption intensity is observed with increasing Ni concentration. This improvement may be attributed to the introduction of localized energy states within the band structure due to Ni^{2+} substitution, which facilitates electronic transitions.

The optical band gap (Eg) can be determined using Tauc's relation:

$(\alpha h\nu)^n = A(h\nu - E_g)$

where α is the absorption coefficient, hν is photon energy, and n = 2 for direct allowed transitions. By extrapolating the linear region of the $(\alpha h\nu)^2$ versus hν plot to the energy axis, the band gap can be calculated. The slight red-shift (movement toward higher wavelength) observed with increasing Ni content suggests band gap narrowing, which may be attributed to enhanced d–d electronic interactions and lattice distortion. Such band gap tuning is advantageous for photocatalytic and optoelectronic applications. Overall, UV–Vis analysis indicates that Ni doping effectively modifies the optical properties of $ZnFe_2O_4$ nanocomposites.

D. FE-SEM Analysis

The surface morphology and microstructural features of pure and Ni-doped $ZnFe_2O_4$ nanocomposites were investigated using Field Emission Scanning Electron Microscopy (FE-SEM), as shown in Figure 2. FE-SEM provides high-resolution imaging, enabling precise observation of nanoscale particle morphology and grain distribution [18].

Pure $ZnFe_2O_4$

The FE-SEM images of pure $ZnFe_2O_4$ reveal the formation of irregular, quasi-spherical nanoparticles with noticeable agglomeration. At lower magnification (Figure 2a), the particles appear clustered due to strong interparticle magnetic interactions and high surface energy typical of ferrite nanomaterials. The higher magnification image (Figure 2b) shows nanosized grains with particle diameters predominantly in the range of ~30–45 nm. The observed agglomeration is attributed to the magnetic dipole–dipole interactions, Van der Waals forces and the high surface-to-volume ratio. The nanoscale morphology confirms controlled nucleation during the co-precipitation process.

0.1% Ni-Doped $ZnFe_2O_4$

Upon incorporation of 0.1% Ni, the morphology shows improved uniformity compared to pure $ZnFe_2O_4$. The particles appear relatively better dispersed, with slightly reduced agglomeration. At higher magnification (Figure 2d), the particle size ranges approximately between ~28–48 nm. The marginal variation in particle size suggests that low-level Ni substitution slightly modifies nucleation and growth kinetics without significantly altering morphology. The particles remain predominantly spherical with homogeneous distribution.

0.3% Ni-Doped $ZnFe_2O_4$

With 0.3% Ni doping, a noticeable increase in particle coalescence and surface roughness is observed. The micrographs reveal more compact and interconnected granular structures. The particle size distribution shifts toward larger dimensions, typically ranging from ~40–65 nm (Figure 2f). The increase in grain size may be attributed to enhanced diffusion and crystal growth during calcination induced by Ni^{2+} substitution. Nickel incorporation likely promotes grain boundary mobility, facilitating particle growth.

0.5% Ni-Doped $ZnFe_2O_4$

At 0.5% Ni concentration, further morphological evolution is evident. The FE-SEM images reveal comparatively larger and more defined polyhedral grains. Some particles exhibit partial coalescence, forming compact clusters. The particle size distribution extends approximately from ~50–90 nm, with occasional grains approaching ~100 nm. The observed growth trend suggests that higher Ni concentration enhances crystallite growth during thermal treatment. Increased lattice distortion and cation redistribution may contribute to grain enlargement.

Overall Morphological Evolution

The FE-SEM results clearly demonstrate that Ni substitution influences the microstructural characteristics of $ZnFe_2O_4$ nanocomposites. A gradual increase in particle size is observed with increasing Ni content, indicating that Ni^{2+} ions play a role in

promoting grain growth kinetics during calcination. The nanoscale particle formation across all compositions is consistent with XRD results, which confirmed nanocrystalline spinel structure. Although agglomeration is present in all samples, it is characteristic of ferrite nanoparticles due to intrinsic magnetic interactions. The tunable morphology achieved through controlled Ni substitution may significantly influence the magnetic, catalytic, and optical properties of the synthesized nanocomposites [19].

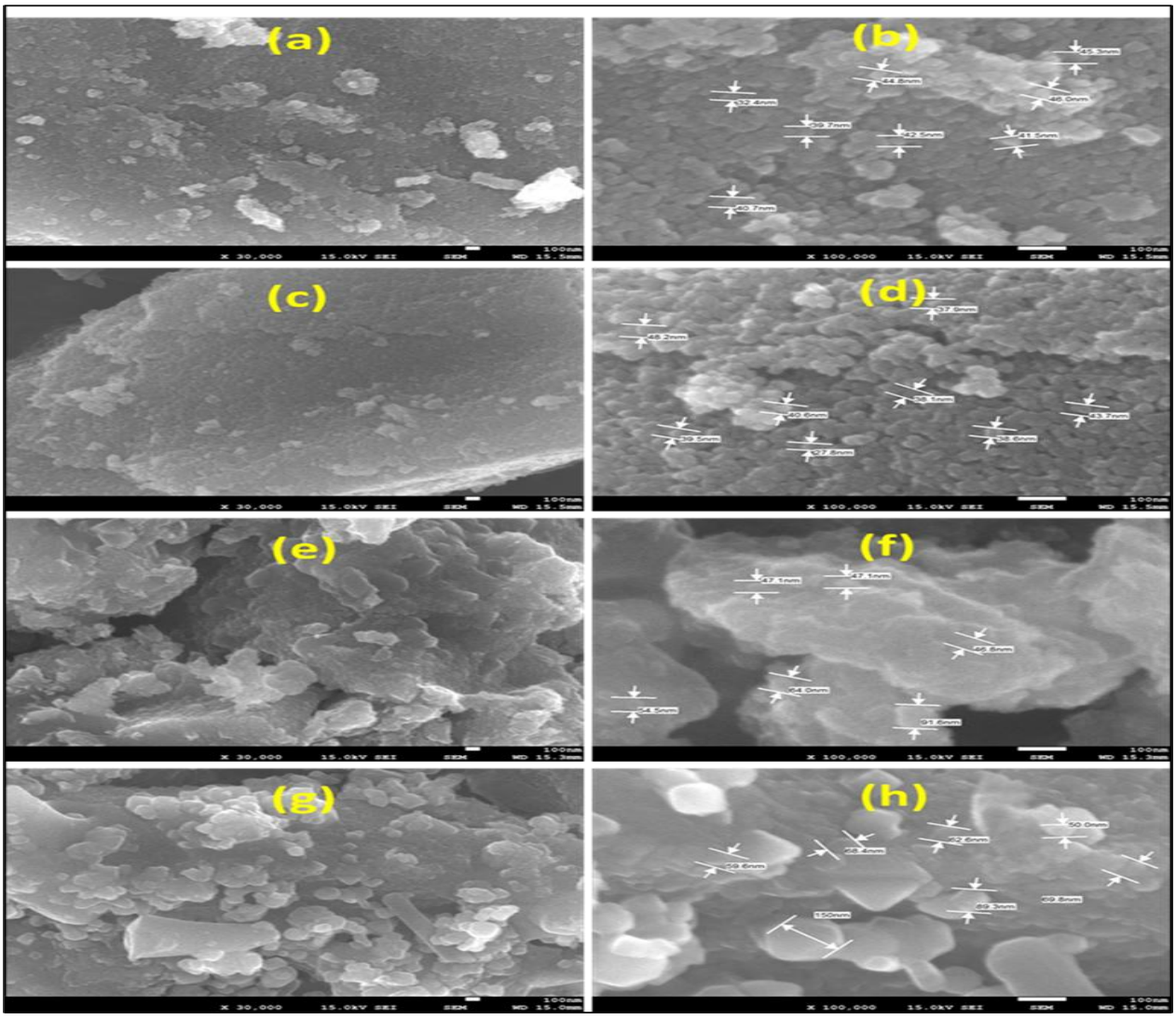

Figure 2. Field Emission Scanning Electron Microscopy (FE-SEM) images of (a–b) pure $ZnFe_2O_4$, (c–d) 0.1% Ni-doped $ZnFe_2O_4$, (e–f) 0.3% Ni-doped $ZnFe_2O_4$, and (g–h) 0.5% Ni-doped $ZnFe_2O_4$ nanocomposites synthesized via chemical co-precipitation method. Images (a, c, e, g) were recorded at lower magnification (×30,000) and (b, d, f, h) at higher magnification (×100,000), illustrating particle morphology and size distribution.

E. EDS Analysis

Energy Dispersive X-ray Spectroscopy (EDS) was performed to determine the elemental composition and confirm the successful incorporation of Ni into the $ZnFe_2O_4$ lattice. The EDS spectra for pure and Ni-doped samples are presented in Figure 3, along with the corresponding quantitative weight percentage (Wt%) values.

Pure $ZnFe_2O_4$

The EDS spectrum of pure $ZnFe_2O_4$ exhibits characteristic peaks corresponding to Fe, Zn, and O,

confirming the formation of zinc ferrite without any extraneous impurity elements. The major peaks observed correspond to:

- O (≈ 0.5 keV)
- Fe (≈ 0.7 keV and 6.4 keV)
- Zn (≈ 1.0 keV and 8.6–9.6 keV)

The quantified elemental composition shows Fe (51.0 wt%), Zn (27.3 wt%), and O (21.7 wt%). The absence of additional peaks confirms phase purity, which is consistent with XRD results. The relative elemental proportions are in reasonable agreement with the theoretical stoichiometry of $ZnFe_2O_4$, considering the limitations of EDS in detecting light elements such as oxygen with high accuracy.

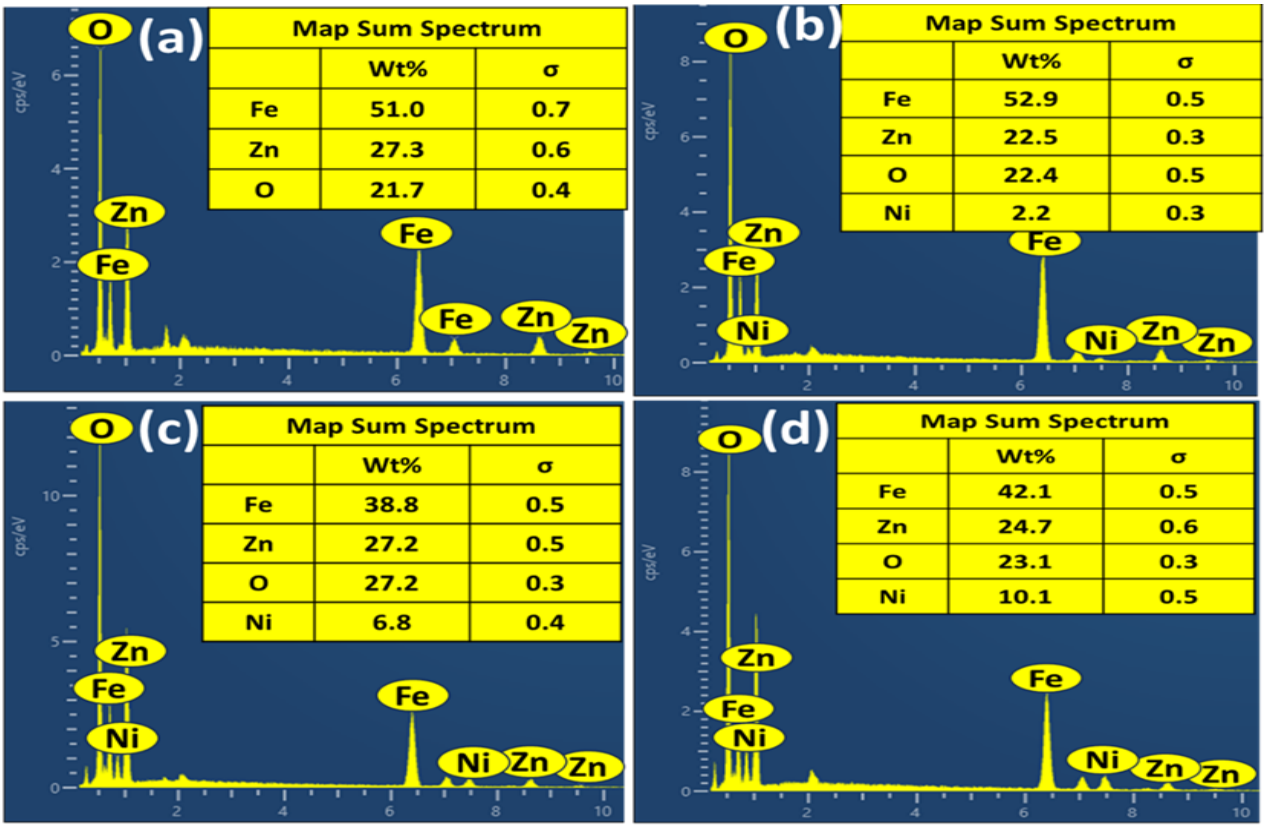

Figure 3. Energy Dispersive X-ray Spectroscopy (EDS) spectra and corresponding elemental weight percentage (Wt%) analysis of (a) pure $ZnFe_2O_4$, (b) 0.1% Ni-doped $ZnFe_2O_4$, (c) 0.3% Ni-doped $ZnFe_2O_4$, and (d) 0.5% Ni-doped $ZnFe_2O_4$ nanocomposites synthesized via chemical co-precipitation method.

0.1% Ni-Doped $ZnFe_2O_4$

For the 0.1% Ni-doped sample, additional peaks corresponding to Ni are clearly visible in the spectrum (≈ 0.85 keV and ≈ 7.5–8.0 keV), confirming successful incorporation of nickel into the ferrite matrix. The quantitative analysis shows Fe (52.9 wt%), Zn (22.5 wt%), O (22.4 wt%), and Ni (2.2 wt%). The presence of Ni and the slight reduction in Zn content indicate substitution of Zn^{2+} ions by Ni^{2+} ions within the spinel lattice. The absence of any secondary phase peaks suggests that Ni is uniformly incorporated rather than forming separate NiO phases.

0.3% Ni-Doped $ZnFe_2O_4$

In the 0.3% Ni-doped $ZnFe_2O_4$ sample, the Ni peak intensity increases compared to the 0.1% sample, indicating higher Ni incorporation. The measured composition shows Fe (38.8 wt%), Zn (27.2 wt%), O (27.2 wt%), and Ni (6.8 wt%). The progressive increase in Ni content accompanied by slight variations in Fe and Zn percentages confirms compositional tuning through controlled stoichiometric substitution. The data demonstrate that Ni concentration increases systematically with doping

level, validating the reliability of the synthesis procedure.

0.5% Ni-Doped $ZnFe_2O_4$

For the highest doping concentration (0.5% Ni), the Ni peak becomes more prominent, and the quantitative analysis reveals Fe (42.1 wt%), Zn (24.7 wt%), O (23.1 wt%), and Ni (10.1 wt%). The increasing Ni weight percentage across samples (2.2 → 6.8 → 10.1 wt%) clearly confirms successful and proportional incorporation of Ni into the $ZnFe_2O_4$ structure. The absence of impurity peaks in the spectra further supports the formation of a single-phase Ni-substituted spinel ferrite.

IV. CONCLUSION

$Ni_xZn_{1-x}Fe_2O_4$ (x = 0.0–0.5) nanocomposites were successfully synthesised via a controlled chemical co-precipitation route followed by calcination, enabling precise stoichiometry and homogeneous cation distribution. XRD analysis confirmed single-phase cubic spinel ($Fd\bar{3}m$) formation without secondary phases, while peak shifts indicated effective Ni^{2+} substitution and lattice distortion associated with cation redistribution. The nanocrystalline nature of the samples was verified from crystallite size calculations. FTIR spectra confirmed characteristic spinel metal–oxygen vibrations, with band shifts evidencing modification of local bonding environments due to Ni incorporation. FE-SEM revealed quasi-spherical agglomerated nanoparticles, with progressive grain growth at higher Ni concentrations. EDS analysis validated compositional purity and successful dopant incorporation. UV–Visible measurements demonstrated tunable optical behaviour with a shift in the absorption edge, indicating electronic structure modification upon Ni substitution.

Overall, controlled Ni doping effectively tailors the structural and optical characteristics of $ZnFe_2O_4$ while maintaining phase stability. The scalability and compositional flexibility of the co-precipitation method make these nanocomposites promising for advanced magnetic and photocatalytic applications.

REFERENCES

[1] Qin, Hong, Yangzhuo He, Piao Xu, Danlian Huang, Ziwei Wang, Han Wang, Zixuan Wang, Yin Zhao, Quyang Tian, and Changlin Wang. "Spinel ferrites (MFe_2O_4): Synthesis, improvement and catalytic application in environment and energy field." Advances in Colloid and Interface Science 294 (2021): 102486.

[2] Ma, Jiabin, Biao Zhao, Huimin Xiang, Fu-Zhi Dai, Yi Liu, Rui Zhang, and Yanchun Zhou. "High-entropy spinel ferrites MFe_2O_4 (M= Mg, Mn, Fe, Co, Ni, Cu, Zn) with tunable electromagnetic properties and strong microwave absorption." Journal of Advanced Ceramics 11, no. 5 (2022): 754-768.

[3] Tiwari, Sudeep, Ruturaj Puranik, Nilima Warade, P. B. Mane, Snehal Haldankar, Anol Mondal, Sudhish Kumar, and Shriganesh Prabhu. "Exhaustive investigation of non-stoichiometric $Zn_{0.5}Ca_{0.5}Fe_2O_4$ nanoparticles for high frequency applications." Ceramics International (2025).

[4] Sanchez-Lievanos, Karla R., James L. Stair, and Kathryn E. Knowles. "Cation distribution in spinel ferrite nanocrystals: characterization, impact on their physical properties, and opportunities for synthetic control." Inorganic Chemistry 60, no. 7 (2021): 4291-4305.

[5] Sahoo, Priyambada, Piyush Choudhary, Suvra S. Laha, Ambesh Dixit, and O. Thompson Mefford. "Recent advances in zinc ferrite ($ZnFe_2O_4$) based nanostructures for magnetic hyperthermia applications." Chemical Communications 59, no. 81 (2023): 12065-12090.

[6] Melegy, Alia A., Yasser K. Abdel-Monem, Farag A. Ali, Nermine E. Maysour, and Ayman M. Atta. "Superparamagnetic Fe_3O_4/ZnO/$ZnFe_2O_4$ nanocomposites for efficient photocatalytic degradation of methylene blue from water under UV light." Scientific Reports 15, no. 1 (2025): 40393.

[7] Guo, Xuan, Haojun Zhu, Mingsu Si, Changjun Jiang, Desheng Xue, Zhihua Zhang, and Quan Li. "$ZnFe_2O_4$ nanotubes: microstructure and magnetic properties." The Journal of Physical Chemistry C 118, no. 51 (2014): 30145-30152.

[8] Bini, Marcella, Marco Ambrosetti, and Daniele Spada. "$ZnFe_2O_4$, a green and high-capacity anode material for lithium-ion batteries: A review." Applied Sciences 11, no. 24 (2021): 11713.

[9] Sharma, Rohit, Prashant Thakur, Pankaj Sharma, and Vineet Sharma. "Ferrimagnetic Ni2+ doped Mg-Zn spinel ferrite nanoparticles for high density information storage." Journal of Alloys and Compounds 704 (2017): 7-17.

[10] Joshi, Seema, and Manoj Kumar. "Effect of Ni^{2+} substitution on structural, magnetic, dielectric and optical properties of mixed spinel $CoFe_2O_4$ nanoparticles." Ceramics International 42, no. 16 (2016): 18154-18165.

[11] Renuka, L., K. S. Anantharaju, S. C. Sharma, Y. S. Vidya, H. P. Nagaswarupa, S. C. Prashantha, and H. Nagabhushana. "Synthesis of $ZnFe_2O_4$ nanoparticle by combustion and sol gel methods and their structural, photoluminescence and photocatalytic performance." Materials Today: Proceedings 5, no. 10 (2018): 20819-20826.

[12] Saaid, Farish Irfal, Muhd Firdaus Kasim, Tan Winie, Kelimah Anak Elong, Azira Azahidi, Nurul Dhabitah Basri, Muhamad Kamil Yaakob et al. "Ni-rich lithium nickel manganese cobalt oxide cathode materials: A review on the synthesis methods and their electrochemical performances." Heliyon 10, no. 1 (2024).

[13] Georgieva, Milena, Dimitar Tzankov, D. Kovacheva, Vencislav Tumbalev, T. Karadimov, A. Setzer, P. Esquinazi, and P. A. Georgiev. "Magnetism vs microstructure in Zn-substituted Ni-ferrite nanocrystalline materials with potential for biomedical applications." Journal of Physics D: Applied Physics 59, no. 2 (2026): 025006.

[14] Dippong, Thomas, Erika-Andrea Levei, Iosif Grigore Deac, Firuţa Goga, and Oana Cadar. "Investigation of structural and magnetic properties of $Ni_xZn_{1-x}Fe_2O_4/SiO_2$ ($0 \leq x \leq 1$) spinel-based nanocomposites." Journal of Analytical and Applied Pyrolysis 144 (2019): 104713.

[15] Niaz Akhtar, Majid, Noorhana Yahya, Abdul Sattar, Mukhtar Ahmad, Muhammad Idrees, Muhammad Hasan Asif, and Muhammad Azhar Khan. "Investigations of Structural and Magnetic Properties of Nanostructured $Ni_{0.5+x}Zn_{0.5-x}Fe_2O_4$ Magnetic Feeders for CSEM Application." International Journal of Applied Ceramic Technology 12, no. 3 (2015): 625-637.

[16] Singh, Alka, Richa Tomar, and N. B. Singh. "Efficient removal of crystal violet dye from water using zinc ferrite-polyaniline nanocomposites." Environmental Monitoring and Assessment 196, no. 6 (2024): 569.

[17] Shahbaz Tehrani, F., V. Daadmehr, A. T. Rezakhani, R. Hosseini Akbarnejad, and S. Gholipour. "Structural, magnetic, and optical properties of zinc-and copper-substituted nickel ferrite nanocrystals." Journal of superconductivity and novel magnetism 25, no. 7 (2012): 2443-2455.

[18] Manikandan, A., J. Judith Vijaya, and L. John Kennedy. "Comparative study of pure and Ni-doped $ZnFe_2O_4$ nanoparticles for structural, optical and magnetic properties." Advanced Materials Research 699 (2013): 524-529.

[19] Hafez, Ghoran Salar, Dashti Maryam Fadaei, Aram Maroofi, Mostafa Shafiee, Hoseinabadi Alireza Zare, Farahnaz Behzad, Mohsen Mehrabi, Ali Jangjou, and Kazem Jamali. "Biosynthesis of zinc ferrite nanoparticles using polyphenol-rich extract of Citrus aurantium flowers." (2020): 20-28.